nature sustainability

Supplementary information https://doi.org/10.1038/s41893-025-01520-0

# Contrasting effects of urbanization on vegetation between the Global South and Global North

In the format provided by the authors and unedited

# Supplementary Information

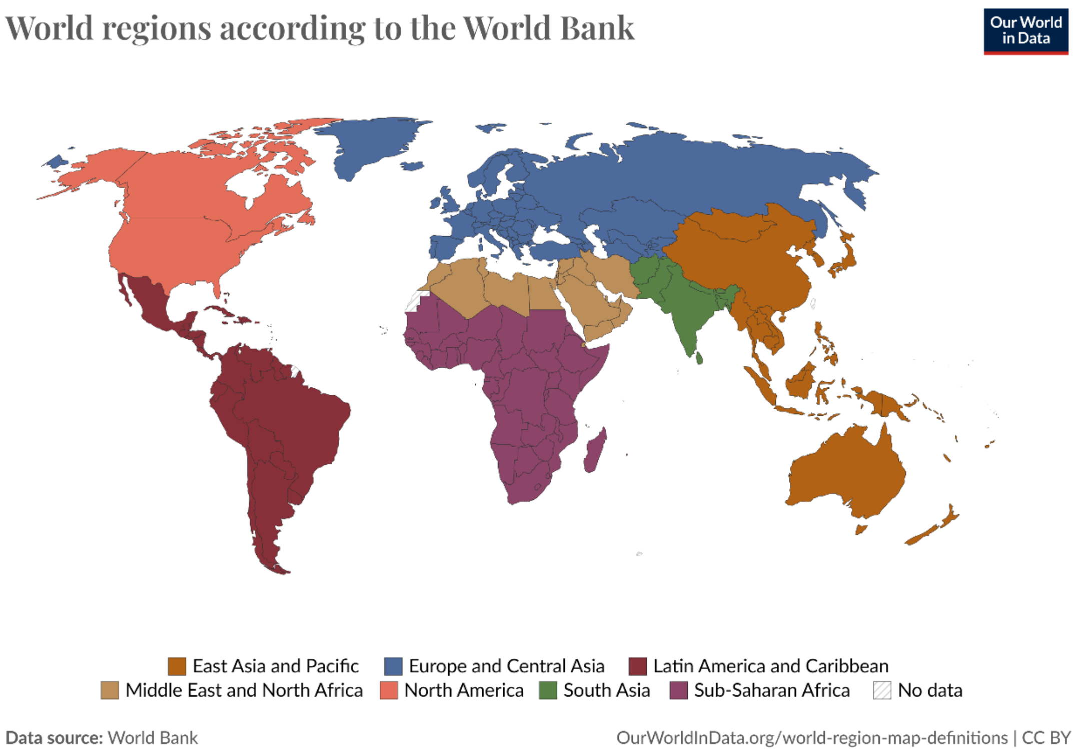


Fig. S1. The seven regions of the world according to the World Bank's division (https://data.worldbank.org/country). The figure is provided by Our World in Data (https://ourworldindata.org/grapher/world-regions-according-to-the-world-bank).

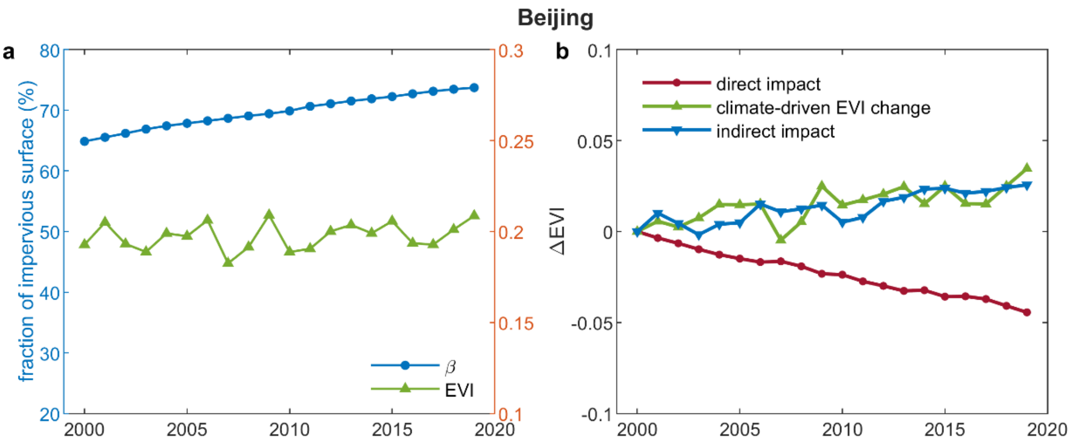


Fig. S2. An example (Beijing, China) for a city experiencing rapid urbanization but greening trend. (a) The annual urbanization intensity ($\beta$), EVI and (b) the direct, indirect impacts on EVI and the macroclimate changes-driven EVI variation during 2000–2019.

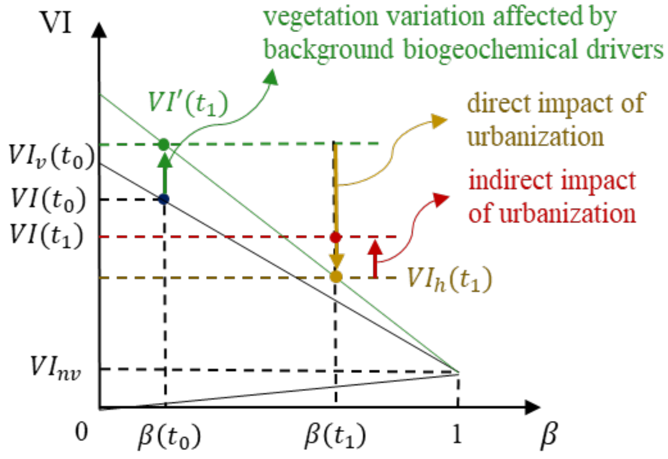


Fig. S3. Schematic diagram of the framework used to separate the direct and indirect impacts of urbanization on the vegetation index (VI) considering the effects of background biogeochemical drivers. $\beta(t_0)$ and $\beta(t_1)$ are the fractions of impervious surfaces at $t_0$ and $t_1$, respectively. The black line is the theoretical linear relationship between the VI and $\beta$ at $t_0$. With changes in background biogeochemical factors, the theoretical linear relationship turns to the green line at $t_1$, and the VI is expected to increase to the green point ($VI'(t_1)$). However, considering the increased $\beta$, theoretically, the VI would drop to the brown point ($VI_h(t_1)$). The difference between $VI_h(t_1)$ and $VI'(t_1)$ is the direct impact of urbanization development. The observed VI ($VI(t_1)$, the red point) is usually different from $VI_h(t_1)$, which indicates the vegetation growth variation driven by urban environment changes and human factors. The difference between $VI(t_1)$ and $VI_h(t_1)$ is the indirect impact of urbanization.

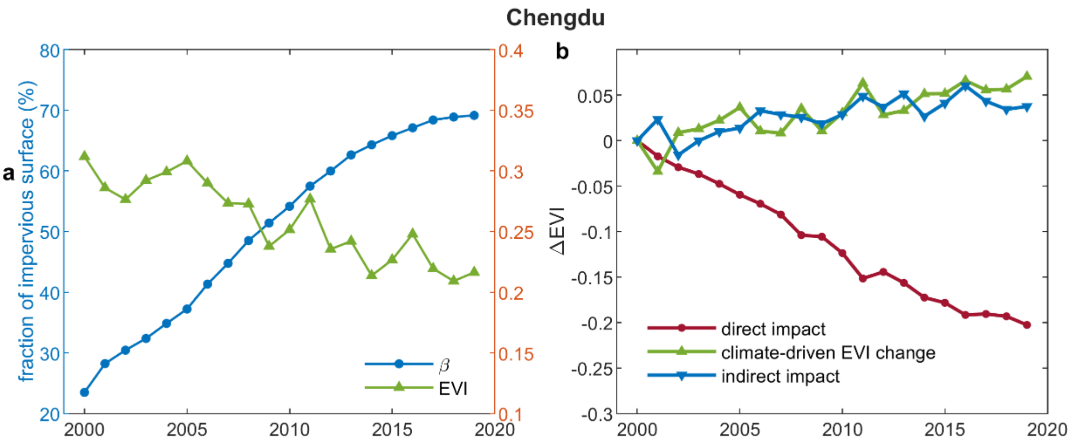


Fig. S4. An example (Chengdu, China) for a city experiencing rapid urbanization and browning trend. (a) The annual urbanization intensity ($\beta$), EVI and (b) the direct, indirect impacts on EVI and the macroclimate changes-driven EVI variation during 2000–2019.

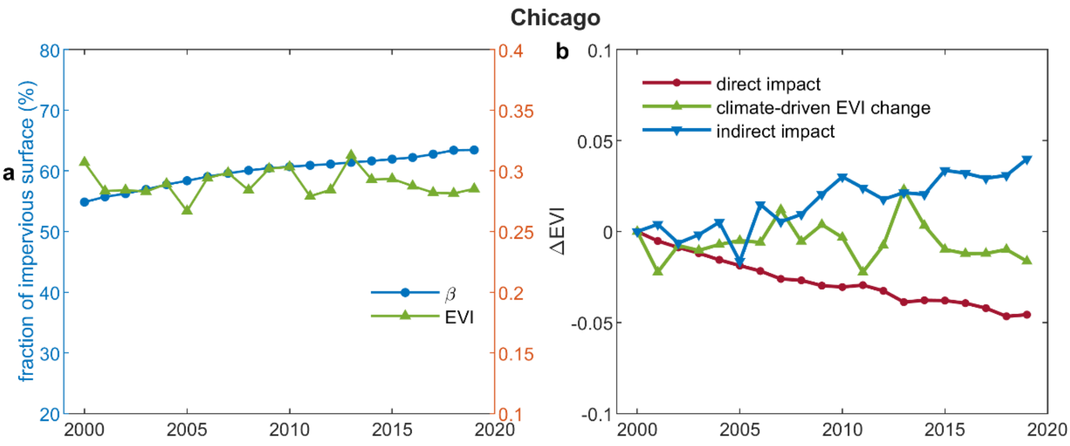


Fig. S5. An example (Chicago, US) for a city experiencing mild urbanization and slight EVI changes. (a) The annual urbanization intensity ($\beta$), EVI and (b) the direct, indirect impacts on EVI and the macroclimate changes-driven EVI variation during 2000–2019.

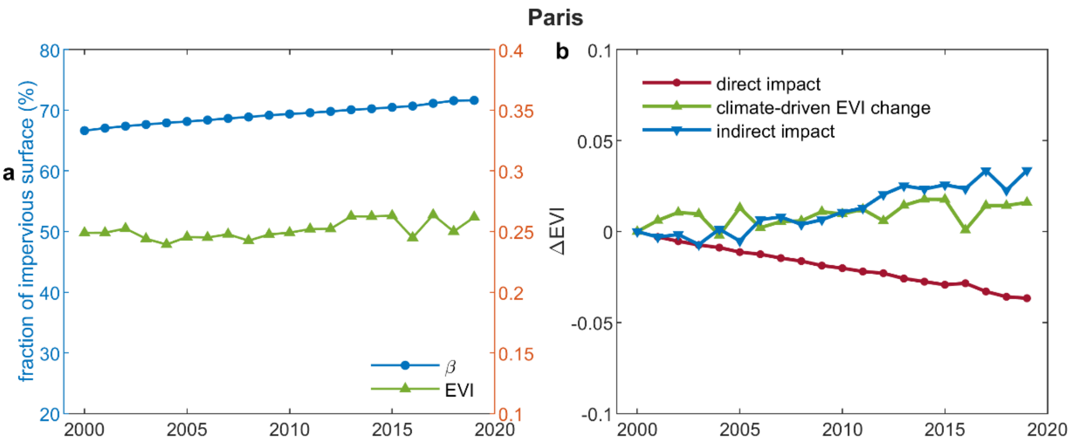


Fig. S6. Another example (Paris, France) for a city experiencing mild urbanization and slight EVI changes in Europe. (a) The annual urbanization intensity ($\beta$), EVI and (b) the direct, indirect impacts on EVI and the macroclimate changes-driven EVI variation during 2000–2019.

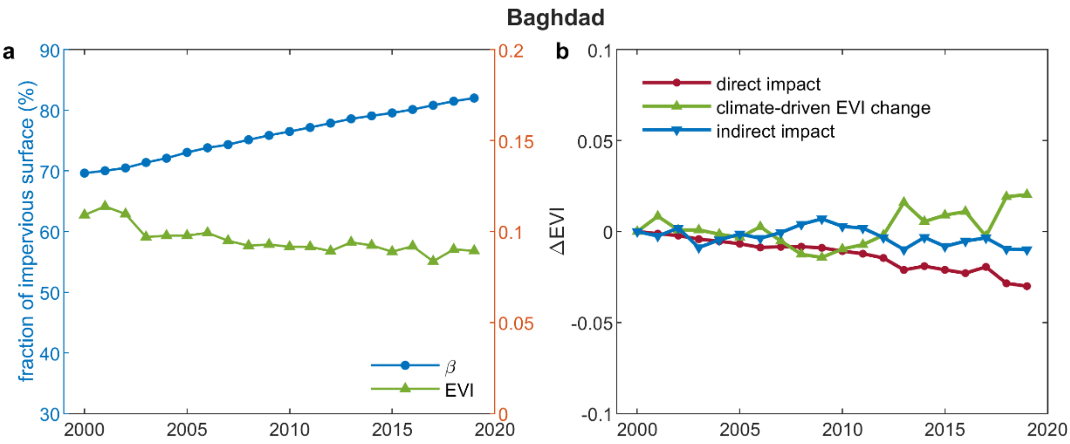


Fig. S7. An example (Baghdad, Iraq) for a city experiencing negative indirect effects of urbanization. (a) The annual urbanization intensity ($\beta$), EVI and (b) the direct, indirect impacts on EVI and the macroclimate changes-driven EVI variation during 2000–2019.

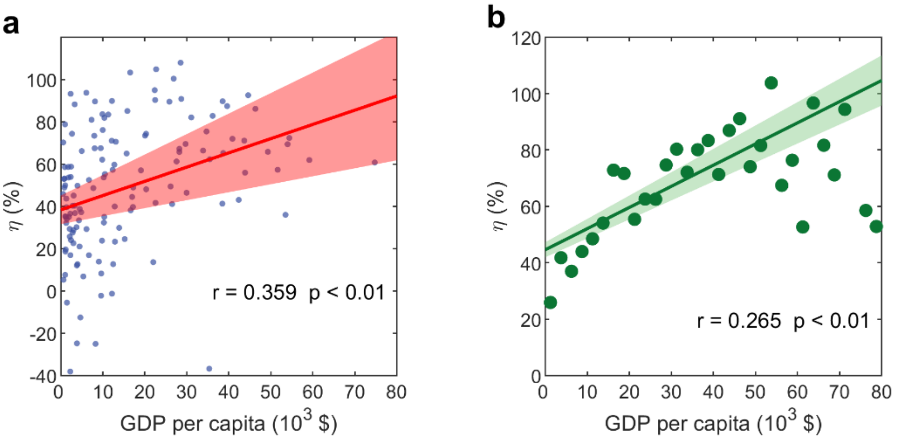


Fig. S8. The effect of economic level on the offsetting coefficient of indirect impact to direct impact of urbanization. a, The relationship between the offsetting coefficient ($\eta$) and GDP per capita at country scale. The solid lines indicate significant trends, and the shaded areas represent 95% confidence intervals. Significance was determined by two-side Student's t-test ($P = 2.4\times10^{-10}$, $n = 139$). b, The relationship between the offsetting coefficient ($\eta$) and GDP per capita at city scale. The $\eta$ values for cities at different development levels are averaged by each 0.025 HDI bin, and each dot represents a bin. Significance was determined by two-side Student's t-test ($P = 6.3\times10^{-77}$, $n = 4718$).

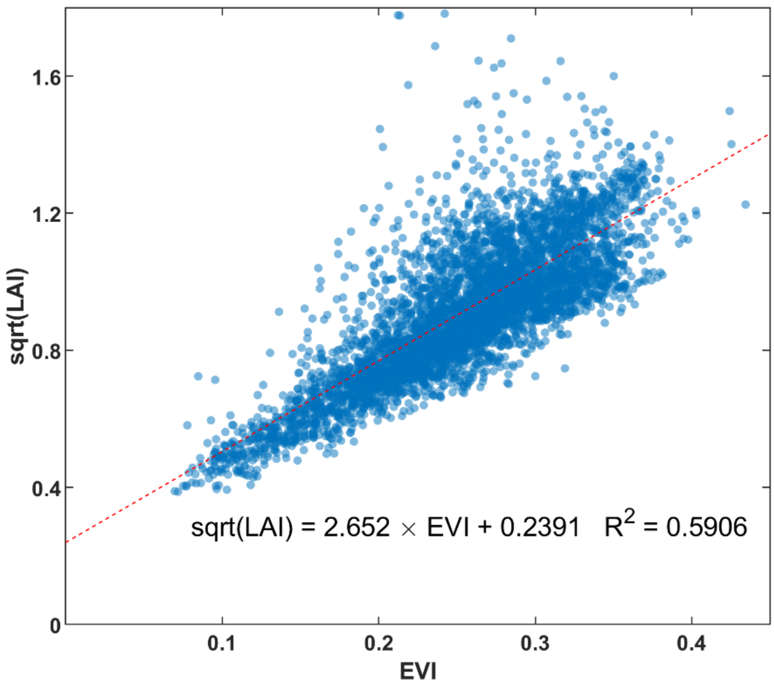


Fig. S9. The relationship between the LAI and EVI of global cities ($P = 1.0\times10^{-255}$, $n = 4718$). Each point represents the EVI and LAI values of a city.

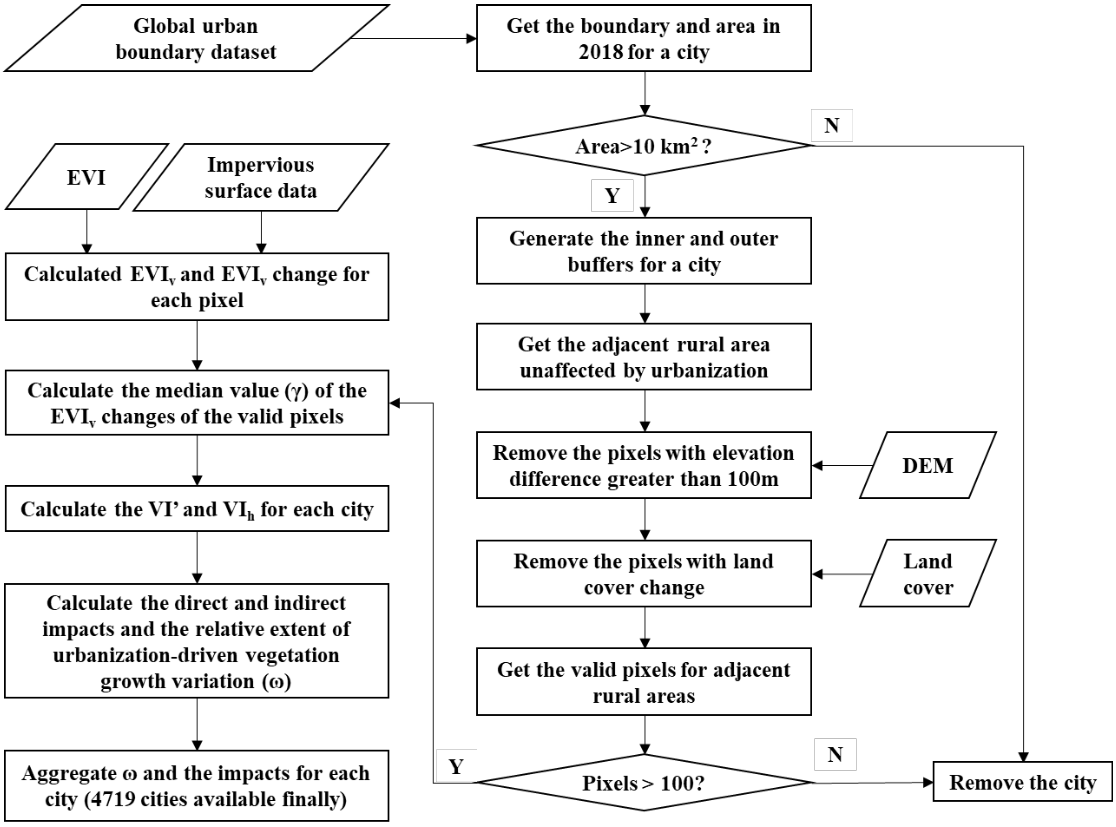


Fig. S10. Flow chart of adjacent substitution method.

**Table S1. Information of CMIP6 ESMs used in this study.**

| Model ID | Institution ID | Resolution (°) | Dynamic vegetation model | Reference |
|---|---|---|---|---|
| BCC-CSM2-MR | BCC | 1.125×1.125 | AVIM2.0 | 53 |
| CanESM5 | CCCMA | 2.8125×2.8125 | CTEM1.2 | 54 |
| EC-Earth3-Veg | EC-Earth Consortium | 0.7031×0.7031 | LPJ-Guess | 55 |
| EC-Earth3-Veg-LR | EC-Earth Consortium | 1.125×1.125 | LPJ-Guess | 55 |
| GFDL-ESM4 | NOAA GFDL | 1.25×1.0 | LM4.1 | 56 |
| INM-CM4-8 | INM | 2.0×1.5 | / | 57 |
| INM-CM5-0 | INM | 2.0×1.5 | / | 57 |
| IPSL-CM6A-LR | IPSL | 2.5×1.2587 | ORCHIDEE | 58 |
| MPI-ESM1-2-LR | MPI-M | 1.875×1.875 | / | 59 |

**Table S2.** Training and cross-validation (CV) correlation of boosted regression tree (BRT) modeling using different combinations of tree complexity, learning rate, and bag fraction. The combination with the highest CV correlation (marked in bold) was used for modeling.

| Tree complexity | Learning rate | Bag fraction | Training correlation | CV correlation |
|---|---|---|---|---|
| 10 | 0.005 | 0.6 | 0.9047231 | 0.7485077 |
| 10 | 0.01 | 0.7 | 0.9247423 | 0.7484487 |
| 10 | 0.01 | 0.8 | 0.9371339 | 0.748394 |
| 10 | 0.01 | 0.6 | 0.9262386 | 0.7477941 |
| 10 | 0.01 | 0.5 | 0.9092262 | 0.7477907 |
| 10 | 0.005 | 0.5 | 0.8930619 | 0.7473129 |
| 10 | 0.005 | 0.8 | 0.9164179 | 0.74728 |
| 10 | 0.005 | 0.7 | 0.9048056 | 0.7471899 |
| 5 | 0.01 | 0.8 | 0.9086596 | 0.7446404 |
| 5 | 0.01 | 0.7 | 0.910305 | 0.7437204 |
| 5 | 0.01 | 0.6 | 0.8997385 | 0.7416203 |
| 5 | 0.005 | 0.8 | 0.8842522 | 0.7412331 |
| 10 | 0.001 | 0.5 | 0.8448382 | 0.741112 |
| 10 | 0.001 | 0.6 | 0.8498364 | 0.740073 |
| 5 | 0.005 | 0.7 | 0.8789196 | 0.7399998 |
| 5 | 0.005 | 0.6 | 0.8763534 | 0.7393476 |
| 10 | 0.001 | 0.7 | 0.8539341 | 0.7390842 |
| 5 | 0.005 | 0.5 | 0.8632926 | 0.7375158 |
| 5 | 0.01 | 0.5 | 0.8781089 | 0.7373064 |
| 10 | 0.001 | 0.8 | 0.857937 | 0.7371554 |
| 5 | 0.001 | 0.5 | 0.7991851 | 0.7234936 |
| 5 | 0.001 | 0.6 | 0.8030141 | 0.7219228 |
| 5 | 0.001 | 0.7 | 0.8059854 | 0.7209028 |
| 5 | 0.001 | 0.8 | 0.8084414 | 0.7197531 |